Interaction of Barotropic Vortices with Coastal Topography: Laboratory Experiments and Numerical Simulations

L. ZAVALA SANSÓN AND G. J. F. VAN HEIJST

Eindhoven University of Technology, Eindhoven, Netherlands

(Manuscript received 18 March 1999, in final form 21 September 1999)

ABSTRACT

The interaction of a barotropic cyclonic vortex on a β plane with a strong topographic slope is studied by means of laboratory experiments and numerical simulations. In the laboratory, the vortex is produced in a rectangular rotating tank with a weak uniformly sloping bottom (slope angle 3.5°) in order to simulate the β effect. The cyclonic vortex moves in the northwestward direction and interacts with an additional, pronounced linear topography (slope angle 35°) along the western boundary of the tank. The laboratory experiments revealed that the original northwestward trajectory changes to the south until the vortex is dissipated by viscous effects and bottom friction. As it moves upslope, the exterior ring of the vortex forms a strong current to the northeast. From this current a new cyclonic vortex is created, repeating approximately the behavior of the original one. Later, two more vortices are formed in the same way.

A finite difference numerical model is used to solve the nondivergent barotropic equation. Despite the presence of the strong slope, agreement between laboratory results and numerical runs suggests that conservation of potential vorticity is indeed the basic mechanism involved in the southward motion of the vortex and the northeastward meandering current.

1. Introduction

Oceanic and atmospheric vortices travel long distances (compared with their size), maintaining a coherent structure. This self-propagation is related with the latitudinal variation of the Coriolis parameter (β effect) while nonlinear effects prevent the vortex dispersion due to Rossby wave radiation. It is well known that cyclonic vortices on a β plane tend to move northwestward, whereas anticyclonic vortices move to the southwest. During their drift, vortices may meet boundaries and interact with them. Because of the direction of propagation, western boundaries are likely candidates for such interactions. However, the problem might be quite different when vortices approach the boundary and experience the presence of the bottom (for example, a continental shelf) before the boundary itself. From the oceanographical point of view, the interaction of oceanic vortices with continental shelves is directly associated with the transport of dynamical and thermodynamical properties of the vortices along the coast. The purpose of this paper is to study the effect of a pronounced western topography on the evolution of a translating vortex on a β plane, by means of laboratory experiments and numerical simulations.

Although real ocean eddies have a baroclinic structure, the barotropic case is considered as a first approximation. The aim is to study the purely topographic effects. The experimental results are restricted to cyclonic vortices due to the difficulty to obtain stable anticyclonic structures in the laboratory. In that case, two- and three-dimensional instabilities are always present (Kloosterziel and van Heijst 1991), which makes the experimental study of their long-term evolution difficult. For this reason, the dynamics of oceanic anticyclonic vortices are studied only by numerical simulations. The vortices are moderately strong [i.e., Rossby number is $O(1)$].

In order to simulate variations of the Coriolis parameter in the rotating tank laboratory configuration, a topographic β plane was adopted: this consists of a weak linear topographic slope, which is dynamically equivalent to the β plane (see e.g., van Heijst 1994). This weak overall topography is present in all the laboratory experiments described below. On a topographic β plane the cyclonic vortices move ''northwestward'' (with the compass directions ''north'' and ''south'' corresponding with ''shallow'' and ''deep,'' respectively). When vortices approach the western boundary they interact with a second linear sloping bottom. The slope of this second topography is in most cases much steeper than that of

Corresponding author address: Luis Zavala Sansón, Fluid Dynamics Laboratory, Dept. of Physics, Building Cascade 2.14, Eindhoven University of Technology, P.O. Box 513, 5600 MB Eindhoven, Netherlands.
E-mail: luis@kiev.phys.tue.nl

the topographic β plane. In addition, the case without this western slope, that is, the purely two-dimensional vortex–wall interaction, is examined (see also Zavala Sansón et al. 1999a). It must be remarked that weak topographies imply small topographic changes compared with the total depth, which is a prerequisite for simulating the planetary β effect correctly. On the other hand, strong topographies imply depth variations of the same order as the total depth, as is the case in the simulation of a western continental slope.

A basic result of the present study is that the barotropic nondivergent model, which filters out gravity waves (see, e.g., Grimshaw et al. 1994a), is good enough to reproduce the laboratory experiments, even with strong western topographies. This important characteristic allows us to explain the main features observed in terms of the dynamics of this quasi-two-dimensional model. By conservation of potential vorticity of fluid parcels, changes in relative vorticity are more dominated by the coastal depth variations than by the (global) β effect. However, the β effect is fundamental because it impels the vortex to move toward the coastal topography. For the case of cyclonic vortices, the interaction with the coastal topography leads to the formation of an intense meandering current along the slope from which new cyclonic vortices are formed. Similar results are found in numerical simulations with parameter values corresponding with typical oceanic eddies and continental slopes.

The meandering behavior of a current flowing northeastward over a western topographic slope, which is a basic result of the present experiments, is discussed in order to give a complete view of the vortex–topography interaction. This phenomenon may also be observed in real, oceanic situations like on the southeast U.S. continental shelf, where the Gulf Stream meanders on and offshore, thus creating frontal eddies (Miller and Lee 1995). In this paper, it is shown that such behavior might be produced by purely topographic effects. These results are reinforced by a simple theory for barotropic jets developed by Cushman-Roisin et al. (1997).

The behavior of an anticyclone approaching a western slope is essentially different. This case is illustrated by numerical simulations using typical oceanic parameters. The main result is the formation of a cyclonic patch, which forms, together with the anticyclone, a dipolar structure moving eastward. Similar results for anticyclonic vortex–topography interaction were reported before by Smith and O'Brien (1983), who performed numerical simulations with a two-layer model, using a linear bottom topography within the lower layer. Smith (1986) performed new numerical simulations with stronger lower-layer, anticyclonic motion. Later, Zavala Sansón et al. (1999b) studied the reflection of barotropic vortices from steplike topographies in laboratory experiments. With regard to the anticyclonic vortex behavior over a western slope, the aim of this paper is only to illustrate the qualitative difference with the cyclonic case and to show that the dipolar structure moving offshore is formed by purely topographic effects in a single layer.

The basic dynamics of the vortex–topography interaction has been studied in different situations, depending on the vortex strength and the topographic slope. As mentioned above, when ignoring lateral boundary effects, an overall weak linear topography is dynamically analogous to the planetary β effect, the upslope gradient being equivalent to the northern direction. This technique of simulating the planetary β effect on the vortex evolution in rotating tank experiments has been applied by a number of researchers (see, e.g., Masuda et al. 1990; Carnevale et al. 1991). These studies have demonstrated the ''northwestward'' drift (upslope and to the left, looking uphill) of strongly nonlinear vortices. On the other hand, by using numerical experiments, Grimshaw et al. (1994b) described the influence of the free surface stretching effects in the cyclone's northwestward drift. Another related study is that of Grimshaw et al. (1994a), who performed numerical simulations of barotropic oceanic eddies on an f plane interacting with hyperbolic-tangent-shaped topographies. They used a spectral model to solve the barotropic nondivergent model (as we shall do with a more simple finite-difference code). An analytical approach shows that both weak and strong cyclonic eddies (with Rossby number $\ll 1$ and ≈ 1, respectively) in a northern hemisphere tend to move inshore and alongshore with the coast to the right because of the slope. Further on it will be shown that the vortices in the experiments follow this rule. Besides, the results of Grimshaw et al. (1994a) for weak cyclones over topography showed coastal trapped waves. Louis and Smith (1982) and LaCasce (1998) also discuss the radiation of topographic waves by weak vortices over a topographic slope. In contrast to previous studies, the present paper aims at gaining a better understanding of the interaction of moderately strong cyclonic vortices with a pronounced western topography, including the β effect, by using experimental evidence and numerical simulations.

The rest of the paper is organized as follows: In the next section the experimental arrangement is presented as well as some typical results of the vortex–topography interaction using a strong western bottom slope. These experiments are compared with the case of the purely vortex–wall interaction on the β plane (i.e., in absence of the strong coastal topography). In section 3 the barotropic nondivergent equations for modeling the experiments are described. In section 4, the results of the numerical simulations reproducing the laboratory experiments are presented. A good agreement between numerical runs and experimental cases allows us to explore some other hypothetical cases; for instance, numerical runs with a larger domain reveal the small influence of the other boundaries and the occurrence of Rossby radiation. Also, it is possible to study a wider range of the parameters involved, including anticyclonic oceanic

cases. Finally, sections 5 and 6 include a discussion and the summary of the results, respectively.

2. Laboratory experiments

a. Experimental arrangement

The laboratory experiments were performed in a rectangular rotating tank ($L_x \times L_y = 100$ cm $\times$ 150 cm) filled with fresh tap water. In all the experiments a standard depth $H_0 = 24$ cm was used and the rotation rate of the tank was fixed at $\Omega = 0.5$ rad s^{-1}, which corresponds with a Coriolis parameter $f_0 = 2\Omega = 1$ s^{-1}. The experimental procedure consisted of setting the tank at the specified constant rotation about 30 minutes before the start of an experiment in order to ensure that the fluid has reached a state of solid body rotation (spin-up).

The planetary β effect was simulated by using a uniform weak linear topography over the length of the tank. For this purpose a false bottom was used, which was lifted $\eta = 9$ cm at one of the ends of the tank; in all cases $\tan\gamma = \eta/L_y = 9/150$, that is, a $\gamma = 3.5°$ slope. This arrangement implies a constant Coriolis parameter f_0 and a smooth linear topography $H(y) = H_0 - y\tan\gamma$. It can be shown that this configuration, the topographic β plane, is dynamically equivalent to a homogeneous oceanic layer with a flat bottom on a β plane (see, e.g., van Heijst 1994), provided the Rossby number of the flow is small enough. In the inviscid limit, conservation of potential vorticity (q) for fluid parcels in the laboratory can be written as

$$q_{\text{lab}} = \frac{\omega + f_0}{H(\text{y})} = \text{const},$$

while in the planetary β plane,

$$q_{\text{ocean}} = \omega + f_0 + \beta y = \text{const}.$$

These relationships show that increasing (decreasing) depth in the laboratory is equivalent to decreasing (increasing) y in the ocean. Then, the shallow part corresponds to the north and the deep part to the south. The experimental β value is given by (van Heijst 1994)

$$\beta = \frac{f_0 \tan\gamma}{H_m}, \tag{1}$$

where $H_m \approx 20$ cm is the mean depth of the tank. In the present experiments $\beta \approx 3 \times 10^{-3}$ (cm s)$^{-1}$. The nondimensional number, which measures the β effect, is

$$\beta' = \beta L/f_0, \tag{2}$$

where L is the horizontal length scale of the vortex. Typical orders of magnitude for vortices in the laboratory are $L \approx 5$ cm (see next subsection) and therefore $\beta' \approx 0.015$. In the ocean, where $\beta \approx 2 \times 10^{-13}$ (cm s)$^{-1}$ and $f_0 \approx 10^{-4}$ s^{-1} for midlatitudes, typical mesoscale vortices have a length scale of order $L \approx 100$ km. Thus, $\beta' \approx 0.02$, which is of the same order as the experimental value.

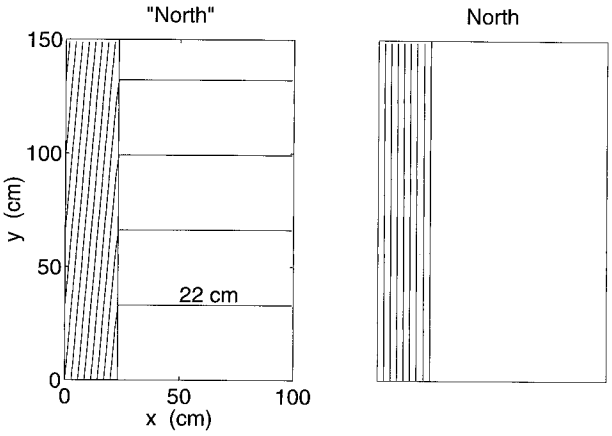

FIG. 1. Left: topographic β plane plus ''coastal'' topography (as used in the laboratory experiments). The interval Δh is 2 cm. Right: planetary β plane plus coastal topography (as used in the numerical simulations).

Besides the weak topography, an additional bottom plate was fixed along the west side of the tank, forming an $\alpha = 35°$ slope with the bottom. This slope, over a width $W = 23$ cm, simulates a continental shelf or strong western topography. Fluid parcels moving on this strong topography effectively experience a different β value because the slope is larger than the overall β topography; besides, the mean depth of the fluid over the coastal topography is much less than in the interior of the flow domain. With $\tan\alpha = 0.7$ and a mean depth $H_S \approx 10$ cm, the topographic β effect of the coastal topography is $\beta_S \approx 7 \times 10^{-2}$ (cm s)$^{-1}$. In nondimensional form, $\beta'_S \approx 0.35$. In order to compare with oceanic cases, consider the continental slope used by Smith and O'Brien (1983), where $\tan\alpha \approx 0.01$ and $H_S \approx 4$ km. Using (1) again, the topographic β effect produced by this slope is $\beta_S \approx 2.5 \times 10^{-12}$ (cm s)$^{-1}$. The nondimensional value is $\beta'_S \approx 0.25$, that is, of the same order of magnitude as the experimental β'_S.

Note that $\beta'_S/\beta' \approx O(10)$ for both, the laboratory and the oceanic cases, which indicates that the vortex evolution will be dominated by the strong topography. Physically, the difference between both systems is shown in Fig. 1. The first plot represents the topography contours of the laboratory arrangement, which consist of both the overall topography (simulating the β effect) and the coastal topography. In this system, the Coriolis parameter is constant. The second picture shows the oceanic case: only the coastal topography is present and the Coriolis parameter changes with latitude. This configuration was used for the numerical simulations (see section 4).

b. Initial condition

In order to produce the vortices, a suction method similar to that in Carnevale et al. (1991) was adopted:

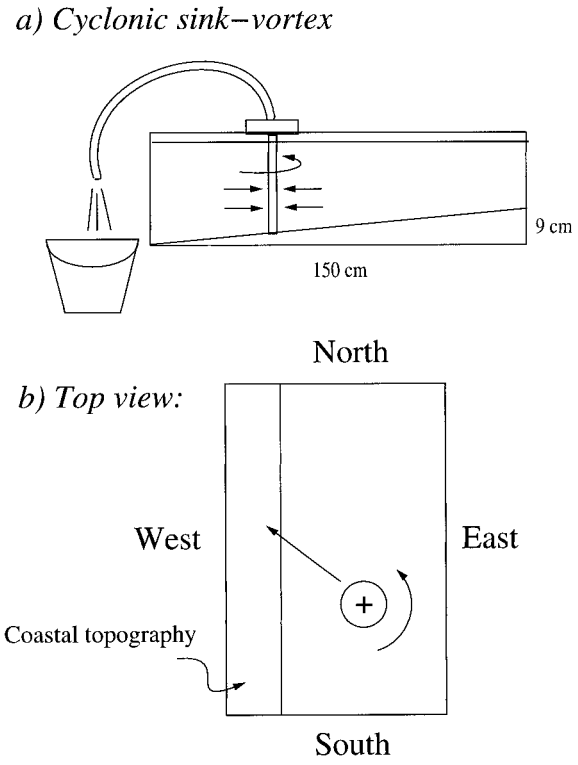

FIG. 2. Initial condition: (a) barotropic cyclonic sink–vortices are produced by syphoning a fixed amount of water. (b) Top view of the initial condition: the vortices move to the northwest approaching the western strong slope.

cyclonic (counterclockwise) vortices are created by syphoning a finite volume of fluid through a thin perforated tube (see Fig. 2). With this method it is possible to reproduce similar initial conditions by syphoning fixed amounts of water during a certain period of time. For the flat-bottom case it was found that, once the forcing was stopped, the vorticity and velocity distributions are well approximated by the following expressions:

$$\omega(r) = \omega_0 \exp\left(\frac{-r^2}{R^2}\right), \tag{3}$$

$$v(r) = \frac{R^2\omega_0}{2r}\left[1 - \exp\left(\frac{-r^2}{R^2}\right)\right], \tag{4}$$

respectively. Here r is the radial distance from the center of the vortex, ω_0 is the maximum vorticity, and R is the horizontal length scale (being the radius at which the maximum orbital velocity occurs). The vortices are nonisolated in the sense that they have a nonvanishing circulation; that is, they contain a nonzero net amount of vorticity. Typical length scale values of the vortices were $R \approx 2$ to 4 cm. The Rossby number of the vortex can be defined as $\text{Ro} = v(R)/f_0R \approx 0.3\omega_0/f_0$. The topographic β effect causes these structures to move in the northwestward direction until they reach strong local topography or a lateral wall.

Initially, the vortices are intense [$\text{Ro} \approx O(1)$] but gradually they decay due to lateral diffusion of momentum and due to bottom friction. The rate of decay induced by a flat bottom is given by the Ekman timescale, defined as $T_E = H/(\nu\Omega)^{1/2}$, where ν is the kinematic viscosity (for water $\nu \approx 0.01$ cm^2 s^{-1} at 20°C). The amplitude of the vortices decays by a factor e^{-1} after one Ekman period. In the present experiments, before the vortices reach the coastal topography (i.e., when vortices only experience the weak slope) the Ekman period is typically $T_E \approx 280$ s for the case of a mean depth $H_m = 20$ cm. However, we must take into account the bottom friction when vortices are interacting with the strong topography. The expression for the Ekman decay timescale on a linear bottom topography can well be approximated by

$$T_\alpha = H_S\left(\frac{\cos\alpha}{\nu\Omega}\right)^{1/2}. \tag{5}$$

For $\alpha = 35°$ and a mean depth $H_S = 10$ cm, the Ekman period is $T_\alpha \approx 128$ s. On the other hand, the rate of decay by lateral diffusion is $T_\nu = R^2/\nu$. In the experiments this diffusion decay timescale measures typically $T_\nu \approx 625$ s. In order to compare the laboratory results with numerical simulations, which do not include bottom friction, the duration of most of the experiments was less than an Ekman period T_α. This restriction is also useful in order to compare the experimental results with oceanic situations, in which the frictional decay associated with the bottom is weaker than in the experiments.

c. Flow visualization

In order to obtain qualitative information, the experiments were visualized by adding fluorescent dye to the vortices; the evolving dye distributions were recorded with a corotating camera mounted at some distance above the rotating tank. On the other hand, quantitative measurements were obtained by tracking passive tracers floating on the free surface. Particle tracking was carried out by using the digital image processing package DigImage (Dalziel 1992). With this technique it is possible to determine the positions and velocities of a large number of tracers and interpolate them onto a rectangular grid in order to calculate the vorticity and velocity fields.

d. Interaction with the strong slope

Figure 3 shows the typical behavior of a cyclonic vortex interacting with the strong western slope. The photographs show top views of the tank, where the upper part corresponds to the ''north'' and the vortex is visualized with dark dye (the domain it is not completely

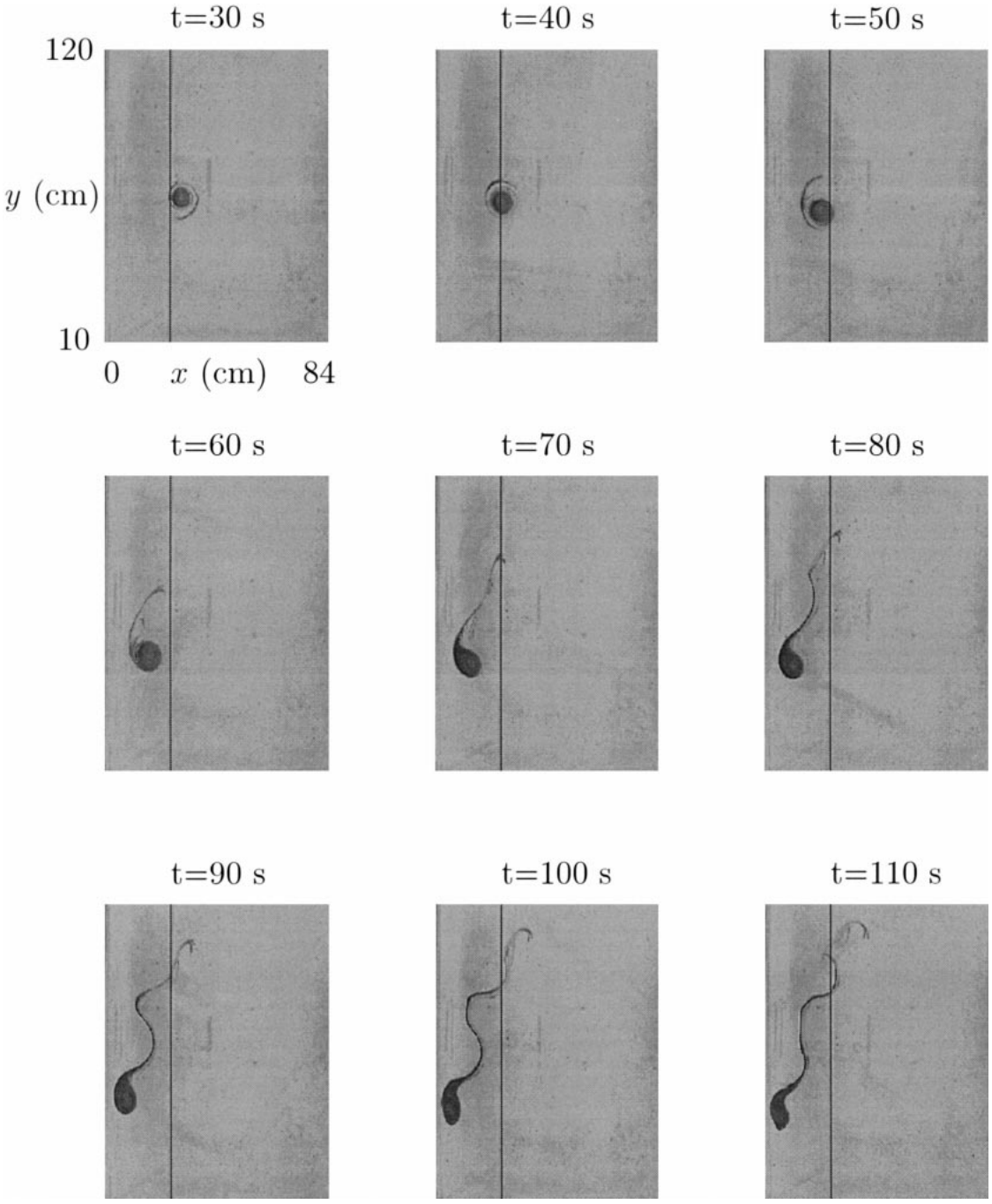

FIG. 3. Top view photographs showing the evolution of the vortex–topography interaction during an Ekman period T_α = 128 s (only part of the domain is shown). The vortex is visualized with dark dye. The western coastal slope starts from the vertical line at x = 23 cm.

visible). Relative to the origin (0, 0) at the southwest corner of the tank, the edge of the western coastal topography lies at x = 23 cm, which is visible in the photographs as a black vertical line. The initial position of the vortex is (x_0, y_0) = (45 cm, 60 cm). In correspondence with the well-known behavior of barotropic cyclones, the initial motion is to the northwest, thus approaching the strong topography. When the vortex interacts with the slope, the following main features are observed: 1) the original vortex changes its trajectory and moves southwestward, until it is dissipated (t = 30–70 s); 2) a growing lobe is created in the northwest part of the vortex (this process starts at approximately t = 40 s), which gradually moves to the north in a

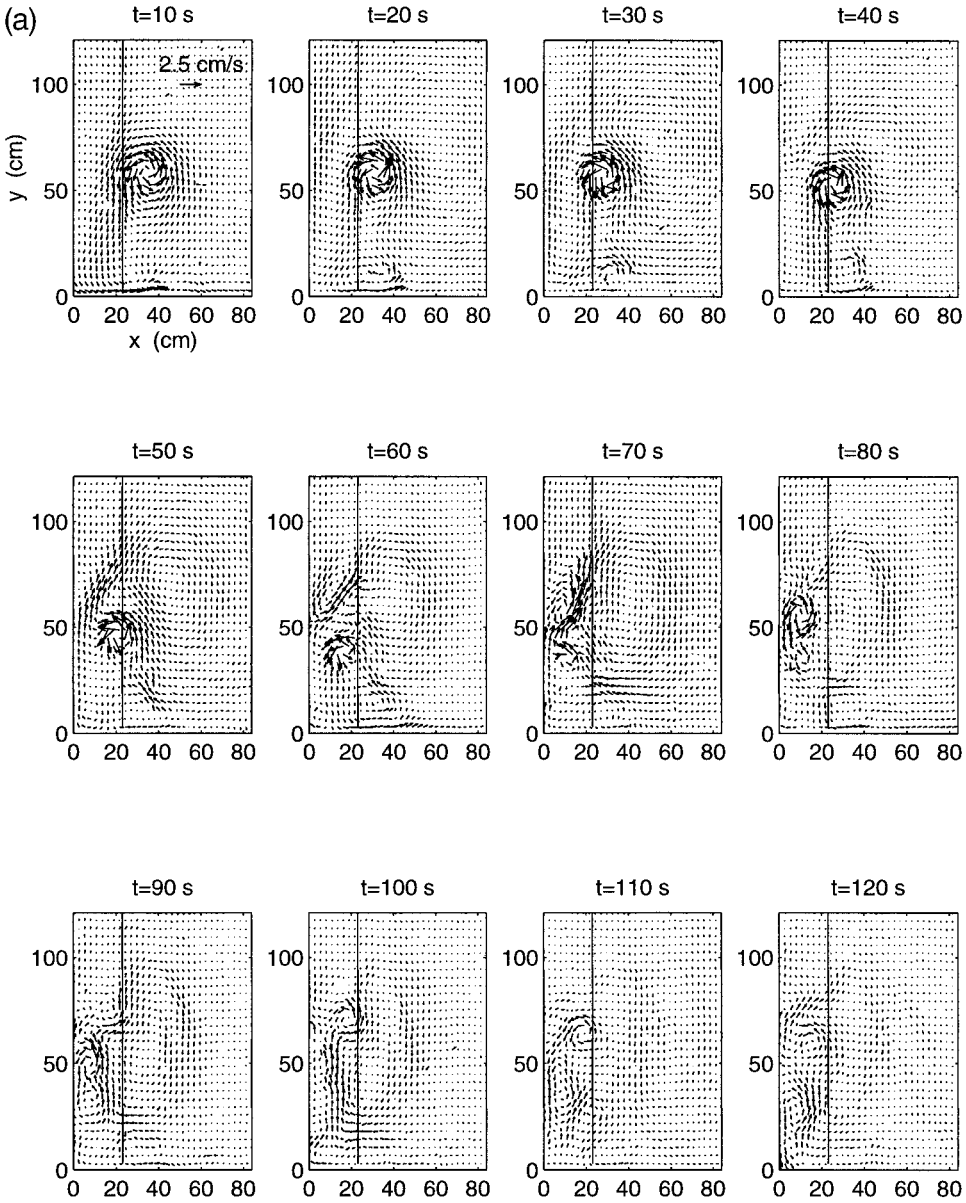

FIG. 4. (a) Velocity fields and (b) streamfunction contours (the interval $\Delta\psi$ is 24 cm^3 s^{-1}; solid (dashed) lines are positive (negative) contours; solid (dashed) lines are positive (negative) contours) of a similar case to that in Fig. 3. The initial vortex parameters are approximately $(x_0, y_0) = (40 \text{ cm}, 60 \text{ cm})$, $R \approx 2$ cm, and $\omega_0 \approx 6$ s^{-1}.

meandering fashion (t = 50–100 s); and 3) from these meanders new cyclonic vortex structures are produced (not visible from this picture since they are formed by undyed, ambient fluid—see below).

From the quantitative measurements we can derive more detailed information about the dynamics involved by plotting the velocity field, interpolated from tracers onto a rectangular grid, as well as the streamfunction field that can be calculated from the velocity data. Figure 4 shows the velocity and streamfunction fields for a case similar to the previous one (shown in Fig. 3). It can be observed that the initial condition produces a southward current along the western wall (t = 10 s), which splits in two parts (t = 20 s): one of them is a northward return flow next to the wall and the other one interacts with the southern boundary creating a small cyclonic vortex. As will be shown further on, the small southern cyclone and the presence of the southern boundary itself are not relevant in the flow evolution. At later stages, when reaching the topography, the original vortex moves to the south and at t = 80 s it is virtually dissipated, as before. Also, observe how a strong current is produced toward the northeast due to the northwest part of the vortex climbing up the strong topography

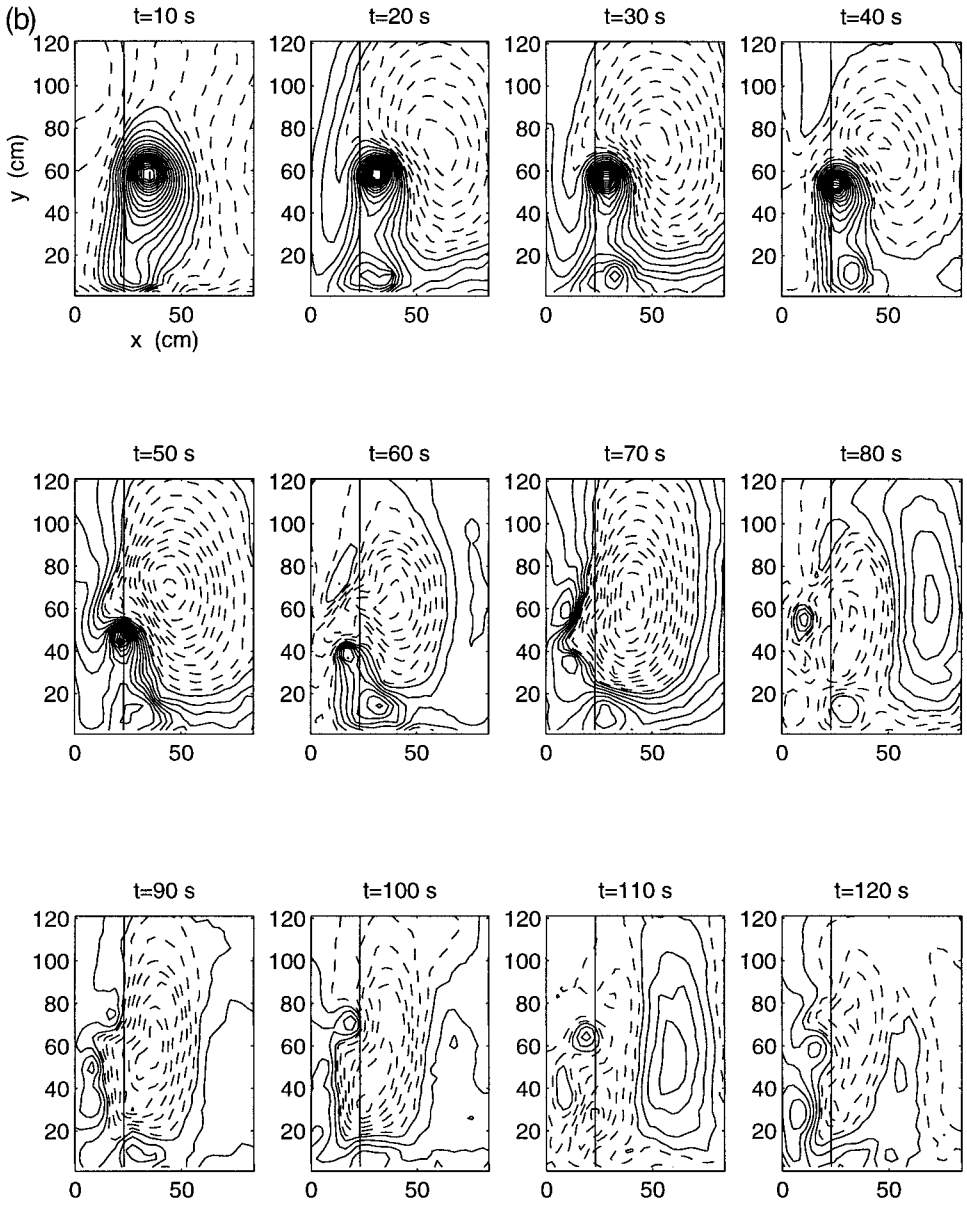

FIG. 4. (*Continued*)

and by the weak return flow next to the wall ($t = 50$ s). This intense current starts a meandering motion that results in the creation of a new cyclonic vortex at $t = 60$ s, and a second one at $t = 90$ s, both moving southward as well. At $t = 120$ s a third cyclonic structure seems to be formed. The dye lobe developed from the vortex in Fig. 3 forms part of this northeastward current and its meandering motion. Note that the new vortices are produced when ambient fluid is surrounded and captured by the meandering current.

Another important characteristic in the experiments is the ''planetary'' Rossby wave radiation by the vortex. An anticyclonic cell covering the whole tank can be clearly observed right from the beginning of the experiment. This cell is associated with the squeezing of fluid columns as they are advected toward the north by the vortex. At $t = 80$ s, a positive cell in the east is created by the opposite mechanism. In order to examine the influence of the Rossby wave radiation and the other boundaries (in particular, the southern wall) on the vortex–topography interaction, several numerical runs were made with different initial positions and larger domain sizes. Qualitatively, the results were similar (see section 4).

The deflection of the original westward vortex motion to the south is more clearly seen in Fig. 5, where the trajectories of two experimental cyclones, starting from a different zonal position, are shown. This behavior is observed when the vortices experience the strong slope.

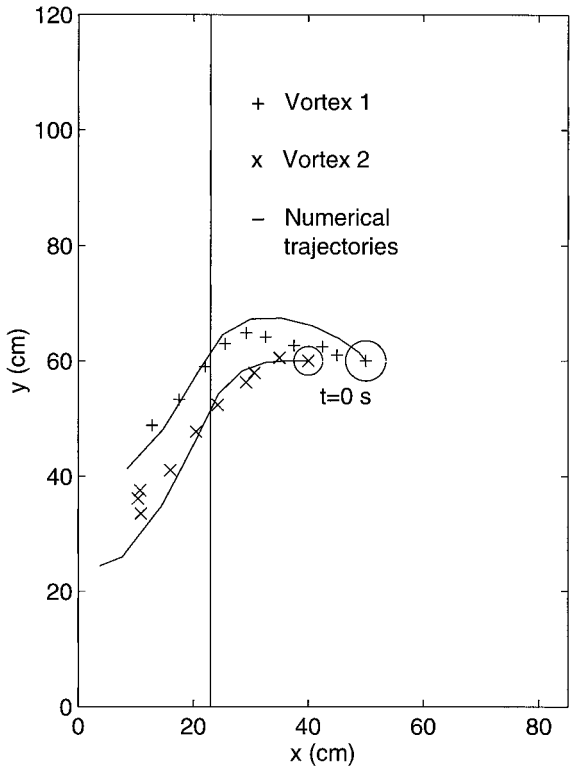

FIG. 5. Trajectories of two experimental cyclones every 10 s (+ and × symbols). The initial vortex positions (indicated with a circle) are $(x_{01}, y_{01}) = (50 \text{ cm}, 60 \text{ cm})$ and $(x_{02}, y_{02}) = (40 \text{ cm}, 60 \text{ cm})$. The solid lines are the corresponding calculated trajectories obtained from numerical simulations during 90 s (see section 4). The initial vortex parameters are $R_1 = 3.5$ cm, $\omega_{01} = 3.5 \text{ s}^{-1}$, and $R_2 = 2.5$ cm, $\omega_{02} = 5 \text{ s}^{-1}$.

Note that the vortex drift is directly to the southwest when the initial position is closer to the coast. As expected, the local topographic β effect induced by the strong coastal slope dominates the weaker β drift induced by the overall topography: the vortex moves towards the ''local northwest'' on the strong slope, that is, to the southwest in the global domain.

e. Vortex–wall interaction

In the absence of the strong coastal topography, but keeping the weak global bottom slope (equivalent to the flat-bottom case on the planetary β plane), the vortex evolution is dramatically different. Figure 6 shows the corresponding fields for a typical case of the vortex–wall interaction. In this type of collision the vortex slightly drifts to the south under the influence of the topographic Rossby wave radiation and the viscous effects at the wall (Zavala Sansón et al. 1999a). A strong current is developed along the coast in the northward direction, which is a well-known leaking effect of a vortex next to a wall: the presence of the boundary blocks the flow and part of it is leaked northward; for an anticyclonic vortex the leaking would be southward (Nof 1988). In the case of stronger interactions (for instance, a more intense vortex or a closer initial position), the viscously produced negative vorticity at the wall is observed to accumulate in a negative eddy, and the vortex then *rebounds* as a dipole structure (see, e.g., Orlandi 1990; Carnevale et al. 1997; Zavala Sansón et al. 1999a).

Thus, in the vortex–wall interaction, the flow evolution depends on the viscous boundary layer next to the wall, unlike the case where the vortex evolution is dominated by changes in depth due to the coastal topography. In section 4, results of a numerical simulation of an intermediate case (i.e., using a moderately strong western coastal topography with a 20° slope) are presented.

3. The physical model

It is assumed that the physical mechanisms involved in the experimental results described in the previous section are governed by the barotropic nondivergent vorticity equation. This is a first approximation of the shallow-water primitive equations for a homogeneous fluid layer over topography (see, e.g., Grimshaw et al. 1994b). Within this approximation the free-surface effects are neglected in the continuity equation, which is equivalent to filtering out gravity waves. In addition, the Ekman damping is not considered. The dynamic equation governing the fluid motion is

$$\frac{Dq}{Dt} = \frac{\nu}{h}\nabla^2\omega, \tag{6}$$

where

$$q = \frac{\omega + f_0 + \beta y}{h}$$

is the potential vorticity, $D/Dt = \partial/\partial t + \mathbf{u}\cdot\boldsymbol{\nabla}$ is the material derivative, $\mathbf{u} = (u, v)$ the horizontal velocity vector with components in x and y directions, $\omega = \partial v/\partial x - \partial u/\partial y$ is the relative vorticity, $\boldsymbol{\nabla}$ is the horizontal gradient operator, ν the kinematic viscosity, $h(x, y)$ the local fluid depth and only depends on the spatial form of the bottom topography, f_0 the Coriolis parameter at a reference latitude, and β its latitudinal gradient. In the inviscid limit, $Dq/Dt = 0$, expresses conservation of potential vorticity per fluid column. The continuity equation is

$$\frac{\partial(hu)}{\partial x} + \frac{\partial(hv)}{\partial y} = 0. \tag{7}$$

Thus, a streamfunction ψ can be defined by

$$hu = \frac{\partial\psi}{\partial y}, \qquad hv = -\frac{\partial\psi}{\partial x}.$$

Then, Eq. (6) is written in the ω–ψ formulation:

$$\frac{\partial \omega}{\partial t} + J\left(\frac{\omega + f_0 + \beta y}{h}, \psi\right) = \nu \nabla^2 \omega, \qquad (8)$$

where J is the conventional Jacobian operator. From the definitions of the relative vorticity and streamfunction it is verified that

$$\omega = -\frac{1}{h}\nabla^2 \psi + \frac{1}{h^2}\nabla h \cdot \nabla \psi. \qquad (9)$$

Note that this model has two dependent variables, namely the horizontal components u and v of the velocity vector because the h field is known from the bottom topography. In this sense the flow is described by a quasi-two-dimensional model. For the flat-bottom case, the flow is purely two-dimensional.

4. Numerical results

The barotropic nondivergent vorticity equation in the ω–ψ formulation, that is, Eqs. (8) and (9), is solved with a finite differences code. It must be remarked that the numerical simulations were performed for flow on a real β plane (with the experimental β value) instead of the topographic β plane used in the laboratory experiments, that is, only the coastal topography was present in the simulations (see also Fig. 1). No-slip conditions were imposed at the lateral flow boundaries in order to simulate the rotating tank experiments.

The aim of the numerical simulations is (i) to demonstrate that the nondivergent barotropic model is able to reproduce the main characteristics of the experimental observations, therefore capturing the basic physical mechanisms in the problem, and (ii) to show that the main experimental results are also found when real oceanic parameters are prescribed in the simulations. Also, numerical simulations of anticyclonic vortices moving to the southwest and approaching a strong western slope are presented in order to illustrate the basic differences with the cyclonic case.

The numerical code was originally developed by Orlandi and Verzicco (see Orlandi 1990) for purely two-dimensional flows and later extended by van Geffen (1998) in order to include rotational effects. In the present study this code is further extended by including topographic effects by means of the barotropic nondivergent model (see also Zavala Sansón et al. 1999b). In this case, the relation between the relative vorticity and the streamfunction is given by Eq. (9) instead of simply a Poisson equation, as in the flat bottom case. A test for the code consisted of comparing simulation results with those of Grimshaw et al. (1994a). They studied the evolution of a barotropic cyclone on a tanh-shaped topography on an f plane. Their plots for the vorticity and the streamfunction distributions were well reproduced by the code. The numerical code was also tested by calculating the evolution of monopolar cyclones on a topographic β plane, and compared with the results obtained by Carnevale et al. (1991). The calculated northwestward trajectories were quite similar to those presented in that paper.

a. Comparison between laboratory experiments and numerical runs

Figure 7 shows a sequence of velocity and vorticity fields of a numerical simulation for approximately the same initial condition of the experimental case shown in Fig. 4. The domain is also a 100 cm $\times$ 150 cm rectangle, discretized by 129 $\times$ 129 grid points. The similarity between the experimental and numerical results is evident in the velocity field sequences. The numerical model reproduces the small cyclonic vortex near the southern wall, the Rossby wave radiation, the weak northward return flow, the northeastward current, its meandering motion, and the creation of new cyclones. It is remarkable that, despite the strong changes in depth on the coastal topography, the main characteristics are well reproduced by the numerical simulations, which are based on the (simplifying) shallow-water approximation. Some differences can be observed after $t = 90$ s; for instance, in the experiments the flow is dissipated faster than in the numerical simulations. These slight differences can be attributed to bottom friction, which becomes more important at shallow parts of the tank, especially close to the western wall.

In order to have a more clear comparison between the experimental and numerical results, Fig. 5 shows the numerically calculated vortex trajectories, together with the corresponding experimental cases already shown. Although the agreement is reasonable, the experimental cyclones appear to drift a shorter distance; most likely this is due to the Ekman decay, which is not present in the numerical simulations. There is also a qualitative difference between the experiments and the simulations, namely, that the experimental vortices are sooner deflected by the coastal slope than in the simulations. This is a consequence of the method by which the vortices were created in the laboratory. Indeed, it takes a few seconds to create a vortex by syphoning water out of the tank; during this time the vortex has already been affected by the topographic slopes. In other words, the initial condition in the experiments is not exactly described by (3) and (4).

The agreement between laboratory experiments and numerical simulations permits one to study the effect of the Rossby wave radiation and the influence of the other lateral domain boundaries by performing the simulation for a larger domain. As it was shown in Fig. 4, the Rossby wave radiation creates a negative cell covering most of the tank; also, a small cyclonic vortex is created next to the southern wall. In order to know how important these flow features are with respect to the evolution of the original vortex, numerical runs were performed for a larger domain (not shown here)

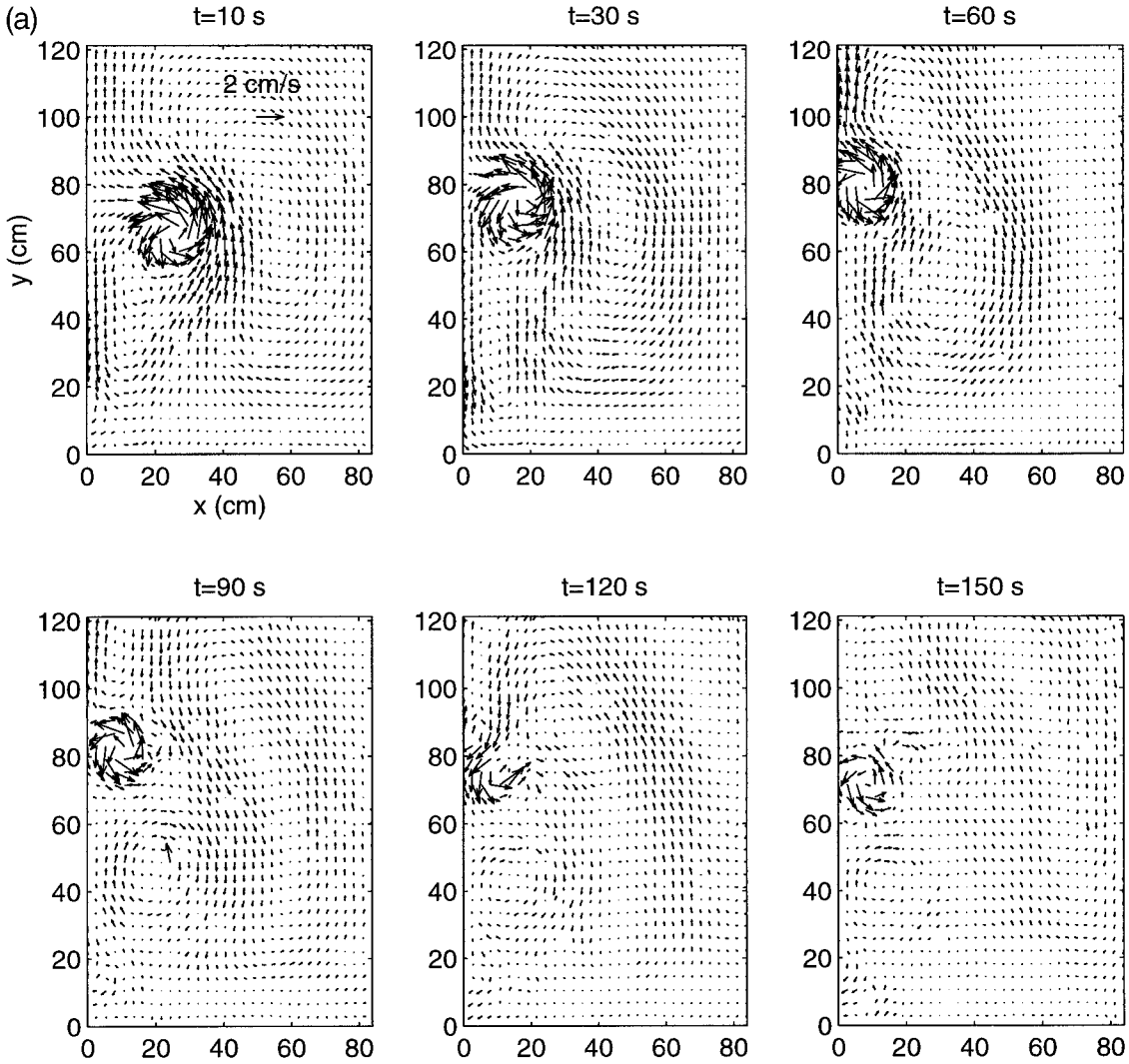

FIG. 6. (a) Velocity fields and (b) streamfunction contours (as in Fig. 4) from a vortex–wall interaction case, that is, in the absence of the coastal topography ($\alpha = 0$). The initial vortex parameters are approximately $(x_0, y_0) = (40$ cm, 60 cm), $R \approx 3.5$ cm, and $\omega_0 \approx 3.5$ s^{-1}.

while keeping the same grid resolution. This large domain was taken as a 200 cm $\times$ 300 cm rectangle (where $0 \leq x \leq 200$ and $-100 \leq y \leq 200$) with 257 $\times$ 257 grid points. The essential behavior was preserved: the vortex moves to the south until it is dissipated, the intense current to the northeast and its meandering motion are produced, and again new vortices are created. Obviously, the small cyclonic vortex produced near the southern boundary in the laboratory experiments is a consequence of the presence of this wall, which is absent in the large-domain numerical runs. As in the real size domain, Rossby wave radiation does not seem to play an important role. Thus, it can be concluded that the size of the tank used in the laboratory experiments does not limit the relevance of the results described before.

b. Case with a less steep slope

In section 2e, experimental results obtained for the case of the vortex–wall interaction were discussed, that is, in the absence of the strong coastal topography (Fig. 6). The differences with the case where the strong topography is present (Fig. 4) are evident (when comparing Figs. 4 and 6, keep in mind that the weak overall topographic slope is always present in the laboratory experiments simulating the planetary β effect). As can be expected, when the coastal topography becomes weaker (smaller slope angle α) the planetary β effect becomes more important with respect to the coastal topography effects, and the vortex interacts more directly with the western wall.

Taking advantage of the fact that the numerical model reproduces the laboratory experiments very effectively

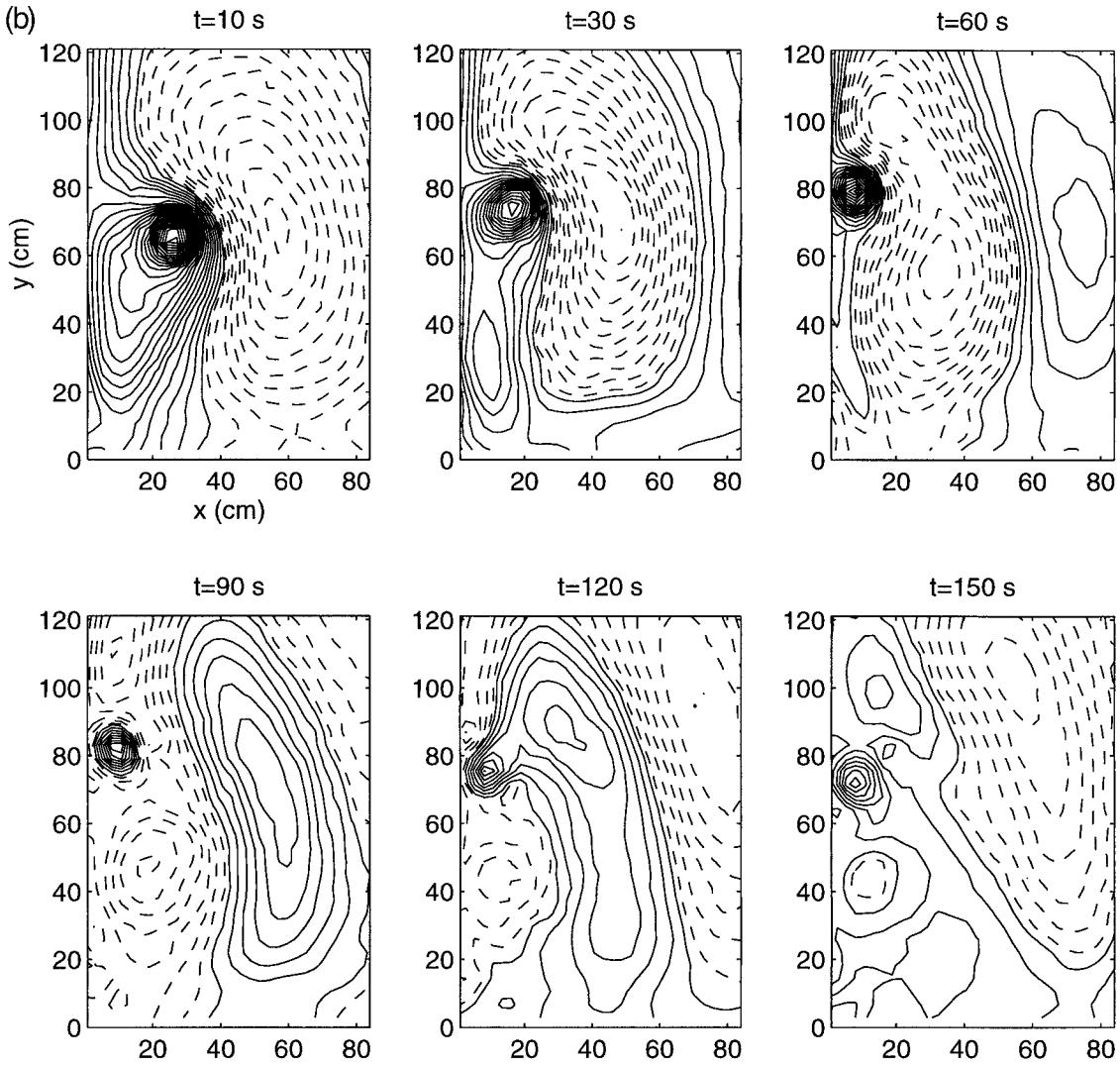

FIG. 6. (*Continued*)

(for times smaller than the Ekman timescale), several numerical runs were performed for decreasing values of the slope angle α in order to investigate the transition to the flat-bottom case. The width of the slope was kept constant (23 cm) and the $\tan\alpha$ value was decreased from 0.7 to 0 (the slope angle was reduced from 35° to 0°). Figure 8 shows the results for the intermediate case $\tan\alpha = 0.364$, that is, a 20° slope. It can be clearly observed that the vortex moves southwestward, but slower than in the 35° case (Fig. 7). At $t = 100$ s this southward drift is almost stopped, and the vortex is gradually dissipated. Note that the vortex is able to get closer to the wall and that it keeps its structure for a longer period. In the purely vortex–wall interaction the vortex was observed to remain almost at a fixed latitude, slowly drifting southward, while leaking fluid (Fig. 6). A northward boundary current is produced at $t = 50$ s by the topographic effect (as in the strong slope case) together with the leaking effect due to the wall (as in the vortex–wall interaction). This northward current separates abruptly from the wall at $y = 80$ cm ($t = 60$ s) and turns downslope (eastward). At $t = 70$–80 s this flow is reinforced as the vortex moves uphill and then produces a new cyclonic vortex at $t = 90$ s, which subsequently moves slowly to the south.

c. Numerical simulations using oceanic parameters

It was already demonstrated that the behavior of the experimental vortices can be reproduced by a simple model as the barotropic nondivergent equation. In this subsection, some examples of numerical simulations using real oceanic parameters are presented in order to compare the experimental observations with large-scale features in the ocean. As mentioned before, the topographic β value associated with the strong topography

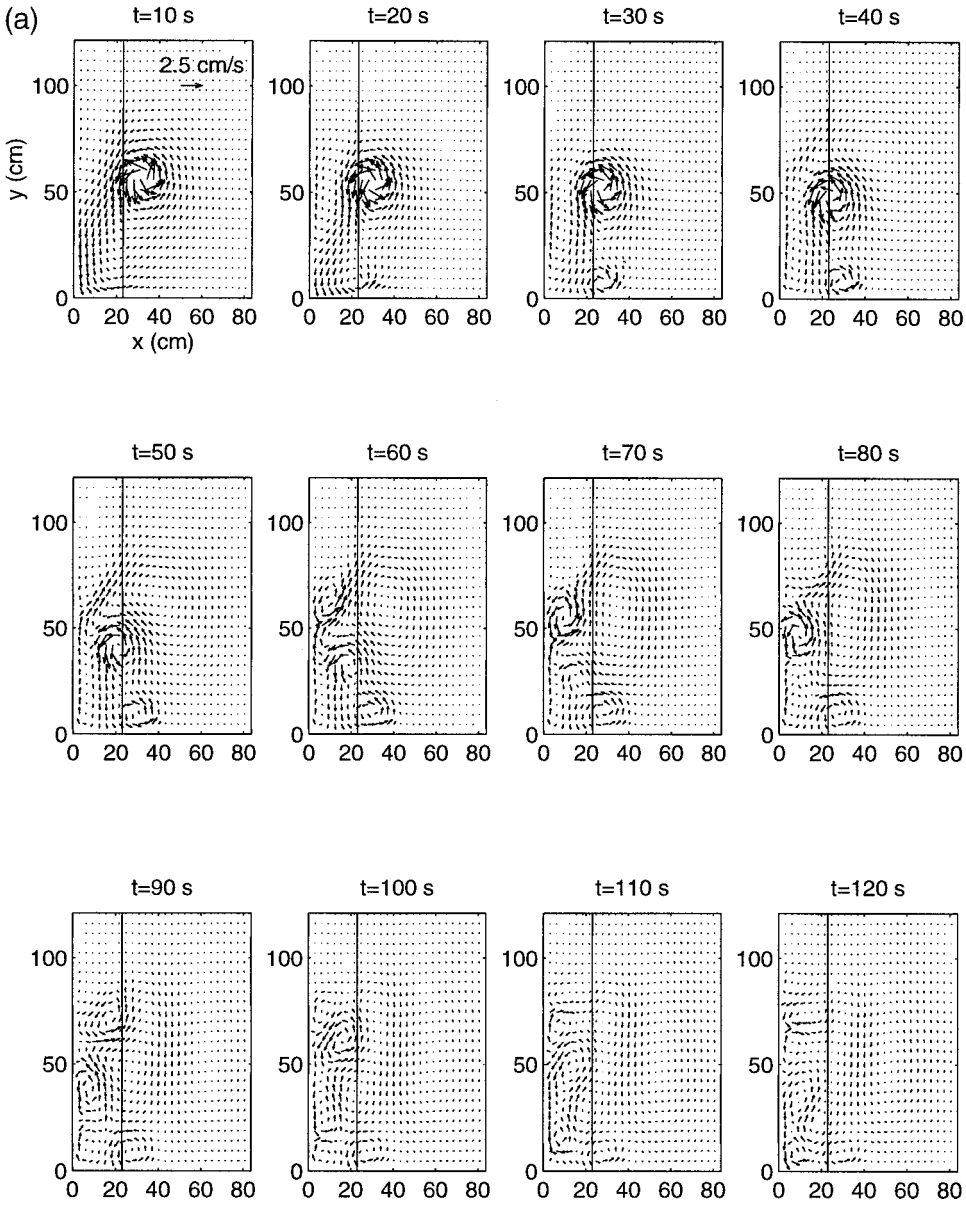

FIG. 7. (a) Velocity fields and (b) vorticity contours (the interval $\Delta\omega$ is 0.15 s^{-1}) from a numerical run similar to that in Fig. 4, now on a β plane, that is, only the coastal topography is included.

used in the laboratory experiments compares very well to that on real continental slopes, and therefore a similar behavior can be expected.

The domain is a 1000 km $\times$ 1500 km rectangle (where $0 \leq x \leq 1000$ and $0 \leq y \leq 1500$). The depth at the western wall is 3000 m and increases linearly up to 5000 m at $x = 333$ km (i.e., the slope is $\tan\alpha = 0.006$ and the mean depth 4000 m). This topography resembles the continental slope of the western part of the Gulf of México (Smith and O'Brien 1983). The eddy horizontal viscosity was chosen as 100 $m^2\ s^{-1}$. The Coriolis parameter was $f_0 = 5.7 \times 10^{-5}\ s^{-1}$ and $\beta = 2 \times 10^{-11}\ (m\ s)^{-1}$. Using these values in (1), the topographic β effect measures $\beta_S = 8.55 \times 10^{-11}\ (m\ s)^{-1}$.

1) CYCLONIC VORTICES

Figure 9a shows the evolution of passive tracers in an oceanic cyclonic vortex of 50-km radius and maximum vorticity $4 \times 10^{-5}\ s^{-1}$. The tracers are placed at $t = 0$ days in a circular ring (with radius 80 km) centered in the vortex. The initial position is $(x_0, y_0) = (500, 750$ km). The vortex tends to move southward under the influence of the slope, while the strong northeastward flow is produced. Clearly, this current is formed from the vortex fluid and it is observed to meander along the slope. In this case, the distribution of the tracers corresponds well with the experimental vortex in Fig. 3. Figure 9b shows the corresponding sequence of vor-

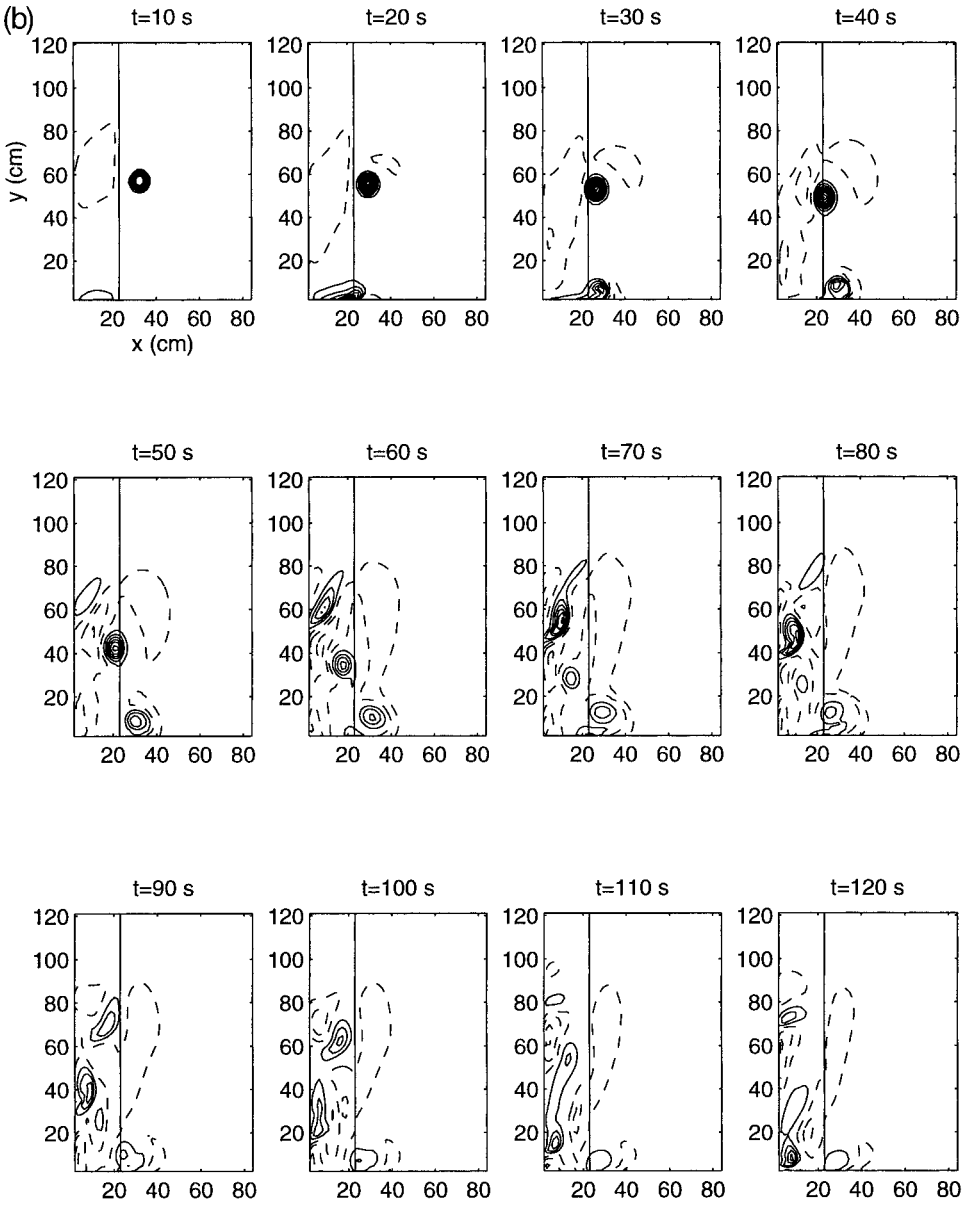

FIG. 7. (*Continued*)

ticity plots. The results show a similar behavior with the experimental observations, although there are some clear differences. The northeastern current is less pronounced than in the experimental case ($t = 20$ days) and only one new cyclone is formed at the slope. Due to its elongated shape, this new vortex does not seem to repeat the behavior of the first cyclone. Another clear difference is the intense vortex activity over the slope, where several cyclonic and anticyclonic cells are formed.

2) ANTICYCLONIC VORTICES

The behavior of an oceanic anticyclone approaching a western slope is essentially different. As in the cyclonic case, Fig. 10a shows the evolution of passive tracers in an anticyclone with the same initial vorticity distribution (with reversed sign) as in the previous case, approaching the western slope from the same initial position. As the vortex moves to the southwest, fluid over the slope is displaced downhill, north of the anticyclone. Due to stretching effects, this fluid acquires positive relative vorticity, which forms a dipolar structure together with the vortex. The pair starts to move eastward until the positive patch is advected southward by the original anticyclone. Note that the vortex leaks fluid southward, but finally is rejected from the slope. For completeness, Fig. 10b shows the sequence of vorticity plots. A relevant conclusion is that the anticyclone cannot reach the slope, as cyclones do. This important char-

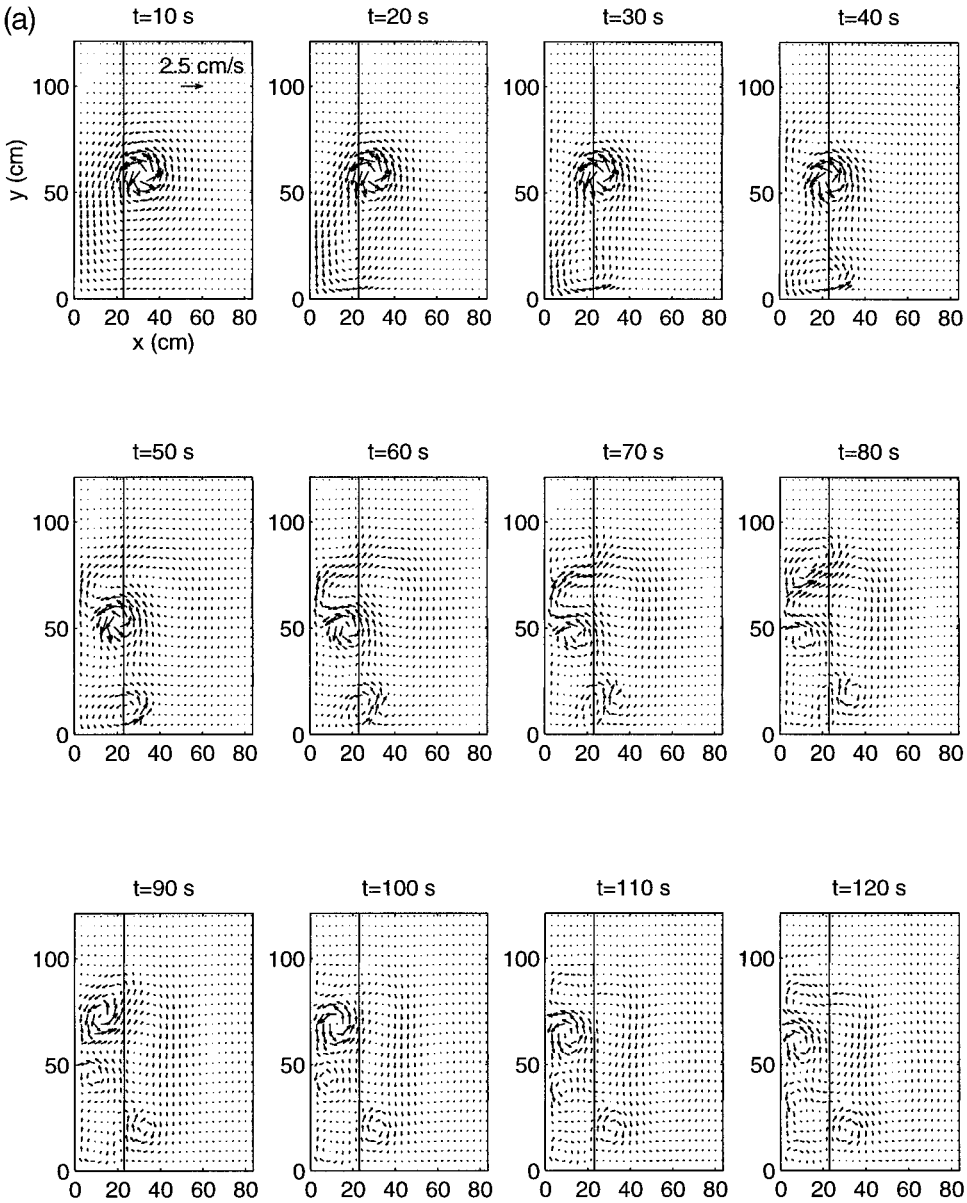

FIG. 8. (a) Velocity fields and (b) vorticity contours (as in Fig. 7) from a numerical run using a less steep western slope ($\alpha = 20°$). The initial vortex parameters are $(x_0, y_0) = (35, 60$ cm), $R = 3$ cm, and $\omega_0 = 2.5$ s^{-1}.

acteristic implies that an anticyclone would be reflected when encountering a pronounced upward slope (see also Zavala Sansón et al. 1999b).

Note from the relative vorticity plots in both cases that the vortices develop a tongue of positive relative vorticity, which forms part of the northeastward current in the cyclonic case and the positive relative vorticity patch inducing the eastward motion on the anticyclone. Figure 11 shows the trajectories of the oceanic vortices approaching the western slope as shown in Figs. 9 and 10. The cyclonic vortex clearly moves as the experimental vortex, while the anticyclone is reflected from the slope, as described above.

5. Discussion

a. The vortex motion

Once it has reached the coastal topography, the cyclonic vortex starts to move southward because the strong topography imposes a local stronger topographic β effect that dominates the global (or planetary) β. These drift motions are shown in Fig. 5 for experimental and numerical cyclonic vortices, and in Fig. 11 for numerical cyclonic and anticyclonic cases where oceanic parameters were used. This general behavior is in agreement with the findings of Grimshaw et al. (1994a), who derived an analytical expression for the initial motion

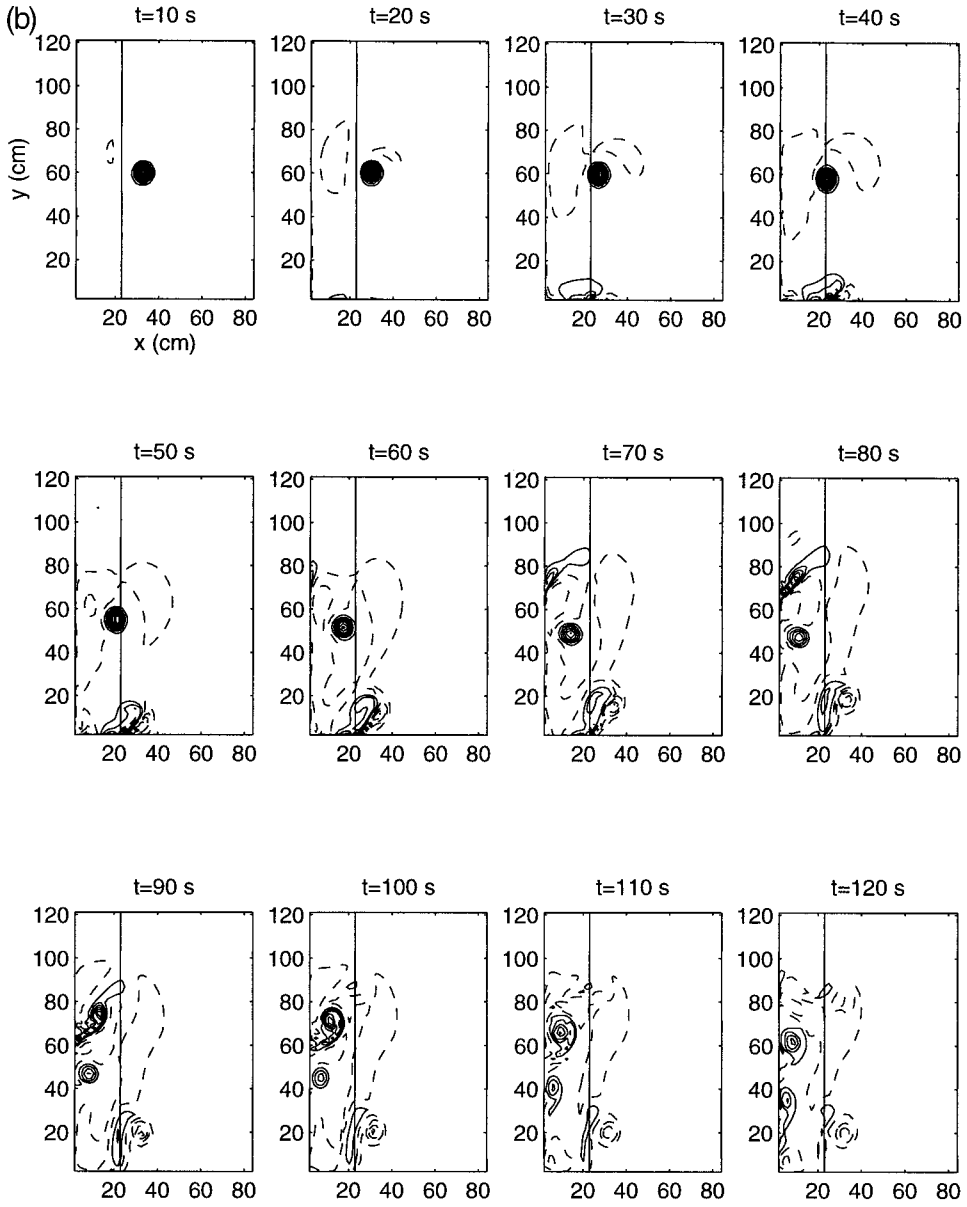

FIG. 8. (*Continued*)

of both weak and strong cyclones in the Northern Hemisphere over a pronounced topography. Despite the strong slope, they showed that the propagation mechanism is essentially the same as that for barotropic vortices on a β plane, at least for the initial stages of motion. In the present case, vortices cannot travel long distances because they lose mass during the interaction with the topography. As it was shown, strong changes in depth induce strong changes in relative vorticity, and advection of the vortex fluid leads to the formation of a pronounced northeastward current. As a result, the vortex is destroyed.

For the case of an anticyclone moving southwest and approaching a western slope, the situation is entirely different. Fluid initially over the slope is displaced downslope, and acquires positive relative vorticity. This oppositely signed vorticity accumulates in a patch, which pairs with the original anticyclone and forms a dipolar structure that moves eastward, that is, away from the coastal topography. The eastward drift resembles the behavior of a modon vortex (see Smith and O'Brien 1983, who found similar results with a two-layer numerical model, and Zavala Sansón et al. 1999b, who described the reflection of barotropic vortices from step-like topographies).

Apparently, the ''northwest'' rule for cyclones applies quite well over the topographic β plane and, for the initial stages of motion, over the strong western slope.

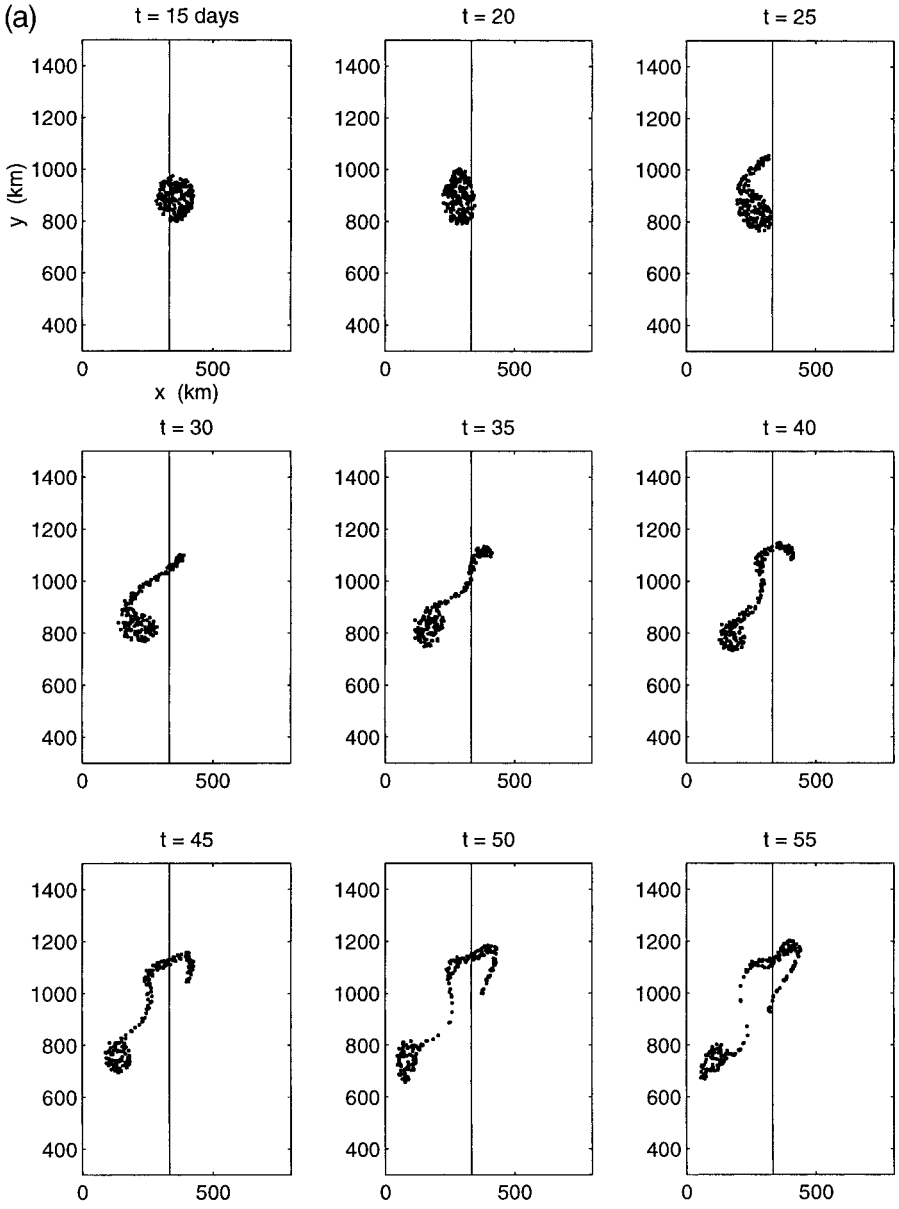

FIG. 9. (a) Tracer evolution and (b) vorticity contours [the interval $\Delta\omega$ is 4×10^{-6} s^{-1}; solid (dashed) lines are positive (negative) contours] from an oceanic cyclonic vortex topography–interaction. The initial vortex parameters are $(x_0, y_0) = (500$ km, 750 km), $R = 50$ km, and $\omega_0 = 4 \times 10^{-5}$ s^{-1}.

It must be noticed, however, that this rule only applies to vortices that are strong enough or to topography slopes that are relatively small in order to avoid the vortex dispersion by topographic Rossby wave radiation. In a recent paper, LaCasce (1998) discussed a way to characterize ''strong'' and ''weak'' slopes in terms of the vortex strength and the slope parameters. Such an effective slope is defined as $\epsilon = \beta L^2/U$, where the topographic β is based on expression (1) and L and U are the vortex length and velocity scales, respectively. The parameter ϵ can be written as

$$\epsilon = \frac{\beta L}{f_0}\frac{f_0 L}{U} \equiv \frac{\beta'}{\mathrm{Ro}}, \tag{10}$$

which is simply the ratio between the nondimensional β effect (see section 2) and the Rossby number. For the experiments in the present paper, $\epsilon \ll 1$ before the vortex reaches the strong slope; in this case the vortex maintains its coherence due to nonlinear effects (moderate Ro) and to low β effect. On the strong slope $\epsilon \approx O(1)$ because the vortex has decayed and, more importantly, β' is larger. During this interaction, apparently,

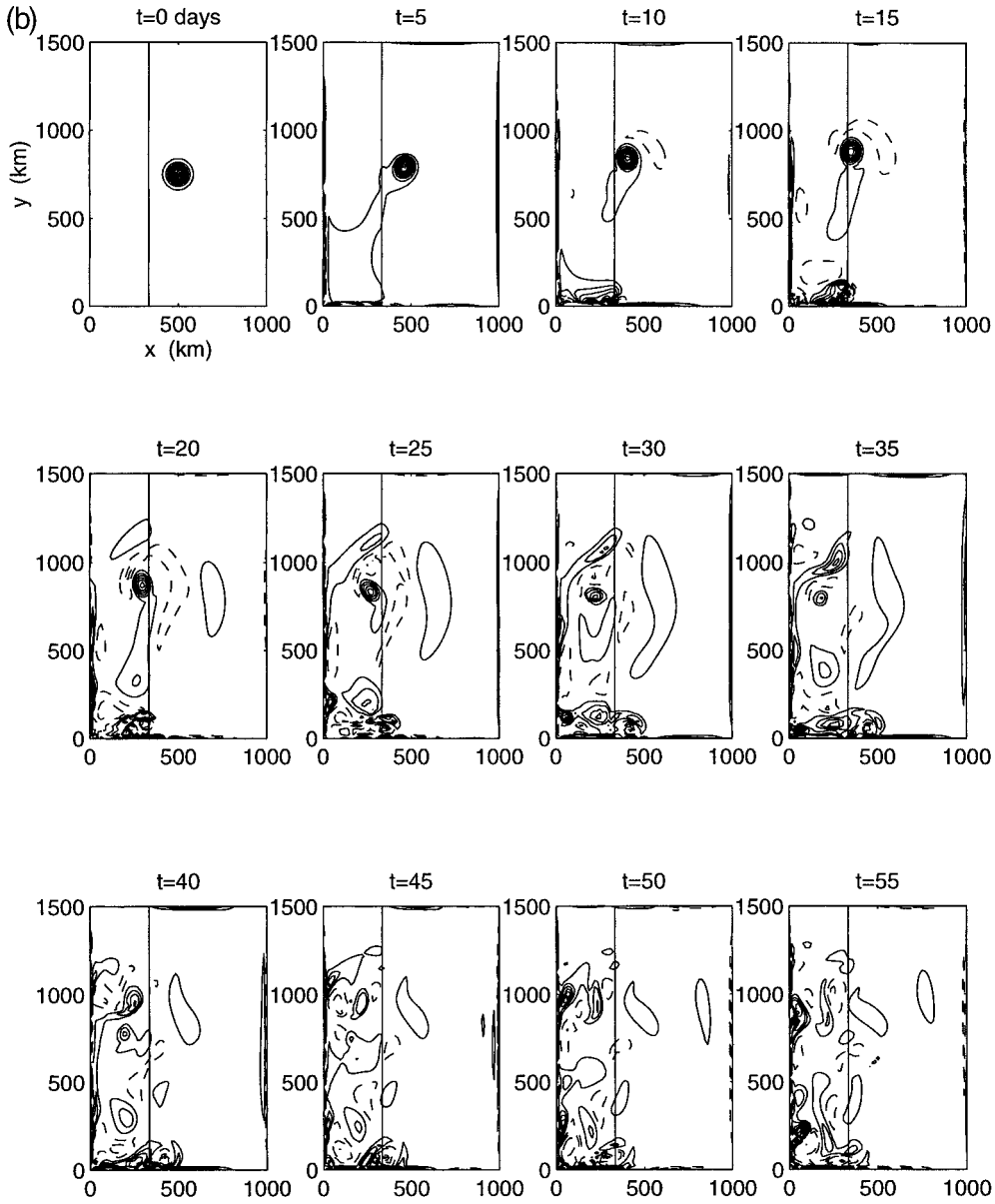

FIG. 9. (*Continued*)

the laboratory experiments are in transition between vortices drifting toward the local northwest and vortices dispersed due to topographic Rossby wave radiation. Although LaCasce (1998) defined the effective slope for a two-layer, quasigeostrophic system on an f plane, his definition provides a suitable way to characterize the vortex–topography interaction in the present experiments.

b. The meandering current

The origin of the northeastward current can be understood in terms of potential vorticity conservation when the vortex experiences strong changes in depth. Fluid columns are squeezed dramatically and relative vorticity is reduced, and may even change sign. In that case, the flow tends to move in clockwise sense. This effect is even more intense when fluid parcels are moving westward, toward the strong topography. Thus, when the vortex moves upslope the northeastward current is clearly intensified (see, e.g., Fig. 4 at $t = 50$ s). The β effect plays an indirect but fundamental role in the formation of this current by impelling the vortex to move toward the coastal topography; that is, the original northwestward motion of the cyclone triggers the formation of the northeastward current.

The northeastward current starts a meandering motion in order to conserve potential vorticity. A physical in-

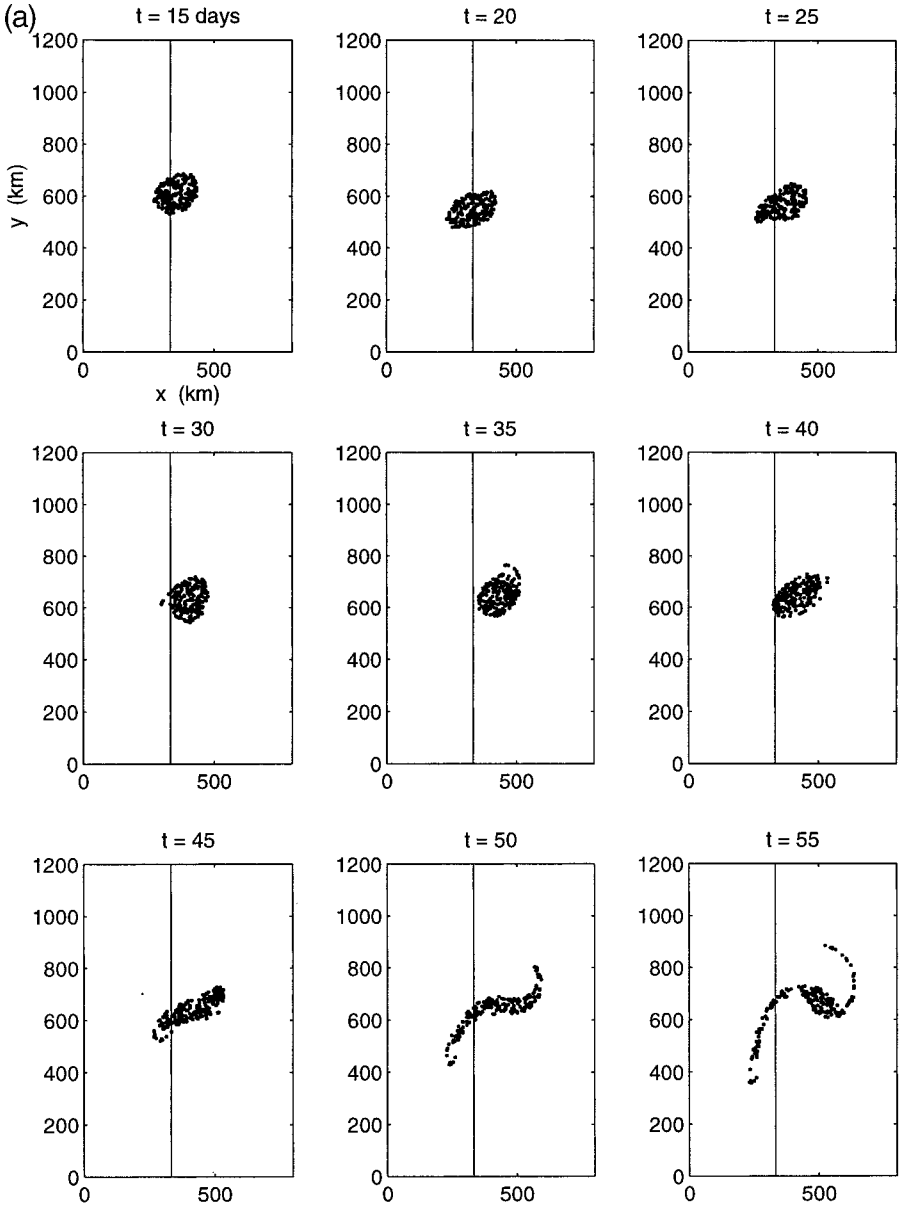

FIG. 10. (a) Tracer evolution and (b) vorticity contours from an oceanic anticyclonic vortex topography–interaction. The initial vortex parameters are $(x_0, y_0) = (500 \text{ km}, 750 \text{ km})$, $R = 50$ km, and $\omega_0 = -4 \times 10^{-5} \text{ s}^{-1}$.

terpretation of this behavior is as follows: when the current moves downhill, changes in relative vorticity are positive and the tendency is to move in an anticlockwise sense. Afterward, the flow moves uphill and fluid columns are squeezed, inducing negative changes in relative vorticity; then, the tendency is now to move in a clockwise sense and the flow turns downhill again. Thus, a meandering jet is produced.

In order to show that this is the physical mechanism that explains the meandering current observed in the laboratory, a simple model for barotropic thin jets over topography is adopted. This model was developed by Cushman-Roisin et al. (1997), although these authors do not present experimental or observational examples. The reader is referred to that article for further details. Although this theory was developed for ideal, narrow barotropic jets, it can be applied to the meandering current formed during the vortex–topography interaction.

Under the assumptions of conservation of volume and potential vorticity, the path equations of a thin jet (compared with the radius of curvature of its trajectory) flowing over an arbitrary topography on an f plane, are

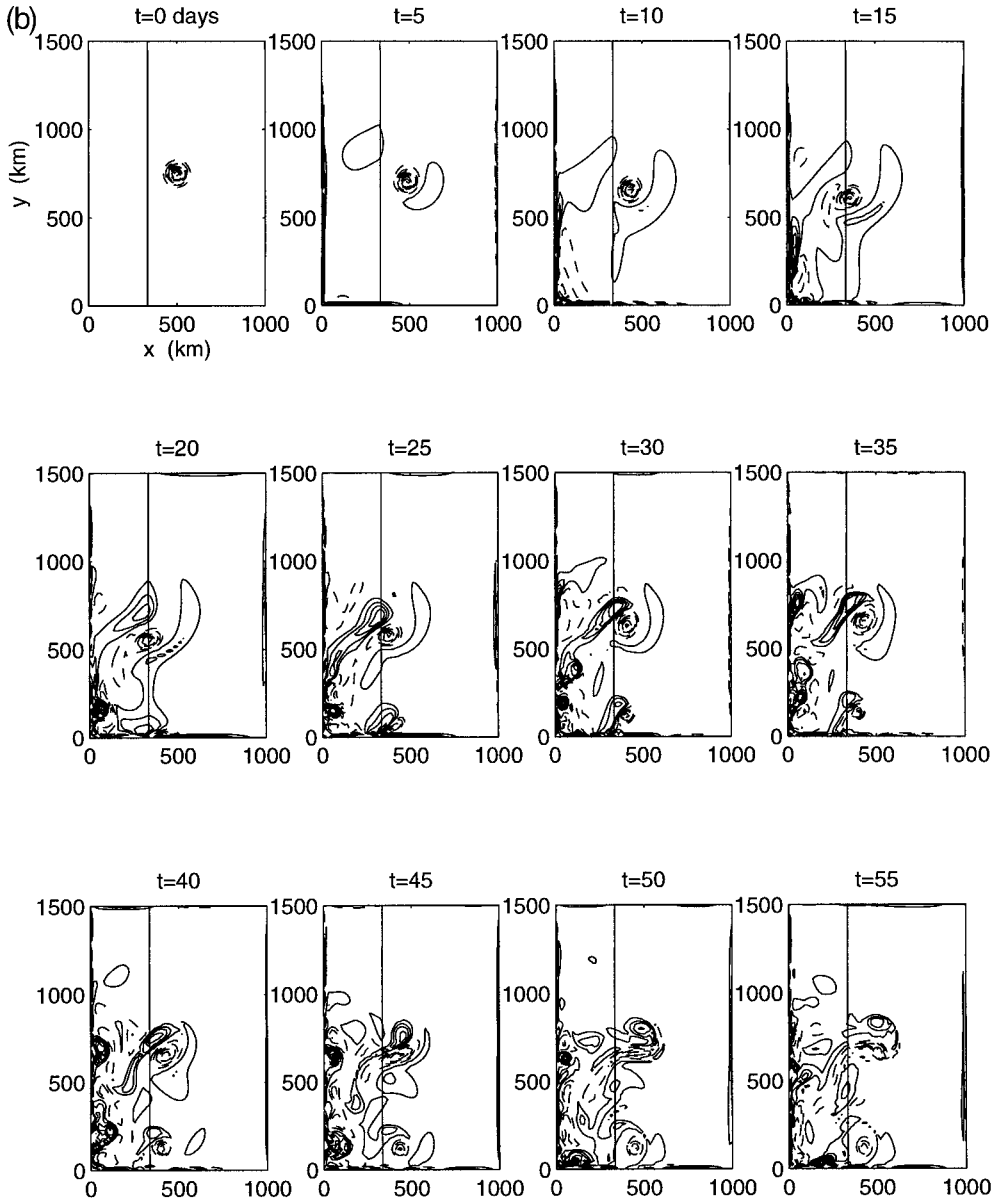

FIG. 10. (*Continued*)

$$\frac{dx}{ds} = \cos\theta \tag{11}$$

$$\frac{dy}{ds} = \sin\theta \tag{12}$$

$$\frac{d\theta}{ds} = \frac{f_0}{U}\left(\frac{h(x, y)}{h_0} - 1\right), \tag{13}$$

where (x, y) are the conventional Cartesian coordinates, s is the coaxial coordinate with the jet, θ is the angle between the jet axis (or the s coordinate) and the x axis, U is the scaled velocity of the jet, $h(x, y)$ is the local depth, and h_0 a reference depth. By integrating this system forward, Cushman-Roisin et al. (1997) studied the trajectories of thin jets over seamounts, ridges, and continental slopes.

In the present case (considering only the coastal topography) the local depth is given by $h(x) = h_p + x \tan\alpha$ for $0 \leq x \leq 23$ cm, and $h = 24$ cm for $x > 23$ cm. The depth at the wall h_p is taken as 8 cm, and the initial depth h_0 is 19 cm. Equations (11)–(13) are integrated using the experimental values of f_0 (1 s^{-1}) and U ($\approx$1 cm s^{-1}). Figure 12 (left) shows the meandering motion of the jet when the initial direction is to the northeast ($\theta_0 = \pi/2 - \phi$ with $\phi = \pi/8$). Also shown is the trajectory of a southeastward jet, which leaves the slope ($\theta_0 = -\pi/2 + \phi$). The size of the meanders is

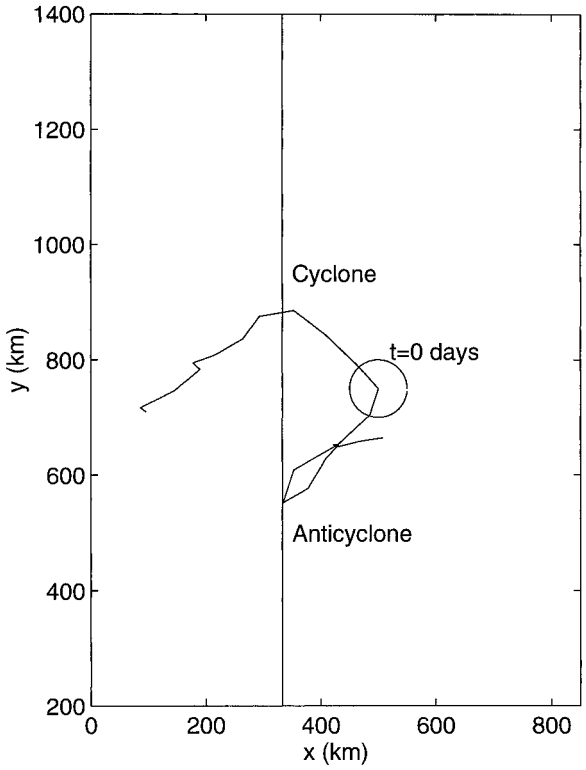

FIG. 11. Calculated trajectories of the oceanic numerical cyclone and anticyclone shown in Figs. 9 and 10, respectively, during 55 days.

estimated by considering small deviations from rectilinear flow along the isobaths, that is, taking $\theta = \pm(\pi/2) + \phi$ with $\phi \ll 1$. The plus (minus) sign corresponds with a northward (southward) jet. From Eqs. (11)–(13) an expression for ϕ can be obtained:

$$\frac{d^2\phi}{ds^2} \pm \frac{f_0 \tan\alpha}{h_0 U}\phi = 0. \tag{14}$$

When the jet flows northward with deep water to the right (positive sign in the second term) the oscillatory motion is produced, with wavelength

$$\lambda = 2\pi\sqrt{\frac{U}{\beta}}, \tag{15}$$

where $\beta = f_0 \tan\alpha/h_0$ measures the topographic β effect [see also (1)]. Using the experimental values, $\lambda \approx 30$ cm, which is in good agreement with the size of the observed meanders. Besides, the new vortices produced from this current have a $\lambda/4$ radius, approximately. When the jet flows southward with deep water to the left [minus sign in (14)], the deviation ϕ grows exponentially and the current leaves the shelf; that is, the mechanism explained above is not able to produce an analogous southward meandering current.

The northeastward motion of the current observed in the experiments is due to the orientation of the isobaths (see Fig. 1). It must also be mentioned that similar meandering behavior was found in the experiments of Baines and Hughes (1996) with a northward boundary

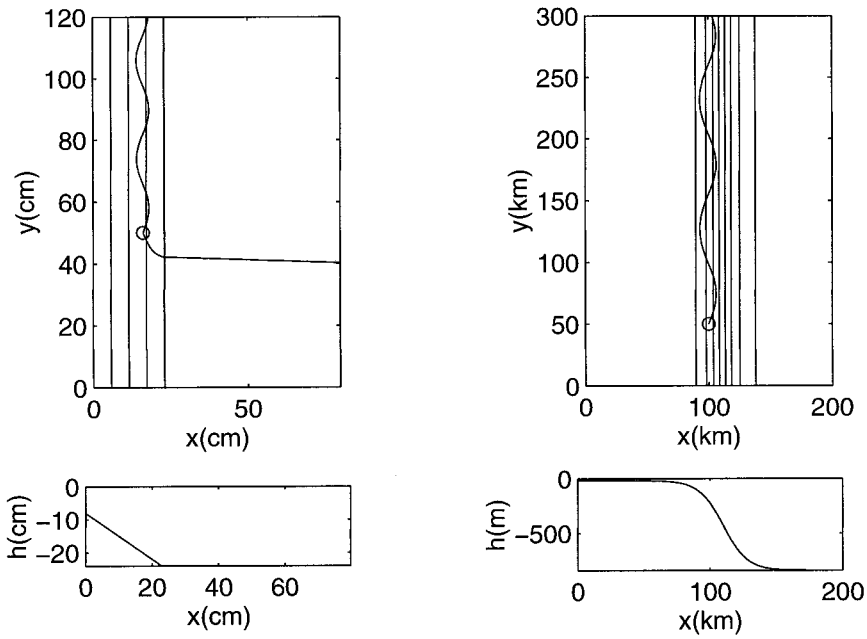

FIG. 12. Left: barotropic jets over the strong topography moving northeastward (meandering motion) and southeastward (the jet leaves the slope), using the laboratory parameters. The paths begin at (16, 50 cm). Right: meandering current over a coastal hyperbolic tangent-shaped topography, using the oceanic parameters given by Miller and Lee (1995). The path begins at (100 km, 50 km).

current on a topographic β plane and with a western slope like in the present study. Their results show that the current separates from the boundary and starts a meandering motion in the northeastern direction.

c. The new vortices

The formation of the new vortices from the meandering current may be considered as a mechanism for the formation of geophysical vortices due to topographic effects. In other words, a cyclonic vortex over strong topography may be able to produce new cyclonic vortices. They arise as a result of the shear between the strong northeastward meandering current and the adjacent fluid. Note that the current contains fluid of the original vortex, while the newly formed vortices contain ambient fluid. Once these vortices have acquired a well-defined shape (slightly elliptical), they repeat approximately the behavior of the original vortex; that is, they move southward.

Similar phenomena have been observed on the southeast U.S. continental shelf, where the Gulf Stream meanders over the topographical slope and elongated cyclonic vortices are produced (Miller and Lee 1995). Figure 12 (right) shows a meandering current moving northward, obtained by solving Eqs. (11)–(13) using the typical parameters in this region ($f_0 = 7 \times 10^{-5}$ s^{-1}, $U = 1.5$ m s^{-1} and $\tan\alpha = 1.5 \times 10^{-2}$), and taking the initial depth as $h_0 = 225$ m. The coastal topography is approximated by a hyperbolic tangent function, similar to that used in the numerical simulations of Miller and Lee (1995). From Eq. (15), the meanders have an approximate wavelength $\lambda \approx 100$ km, which is somewhat lower than the observed value (150–200 km), although of the same order of magnitude. Miller and Lee (1995) discuss the formation of the vortices as a result of hybrid baroclinic–barotropic instabilities. However, the present study shows that such effects might be produced in purely barotropic flows over a pronounced topographic slope.

6. Conclusions

Based on laboratory experiments and numerical simulations it is concluded that a barotropic cyclone moving in the northwestward direction on a β plane and interacting with a strong western linear bottom topography moves southwestward due to the local, intense β effect imposed by the coastal topography. As the vortex moves uphill on the strong slope, an intense northeastward current is developed, which starts a meandering motion by the effect of the topography. This current is formed with fluid from the vortex. New cyclonic vortices are created as the meandering current captures ambient fluid along its northeastward motion. The long-term flow evolution is affected by bottom friction.

The experimental observations are well reproduced by a numerical model based on the barotropic nondivergent equation. Under this approximation the basic mechanism in the vortex–topography interaction is the stretching–squeezing effect on fluid columns as they move through isobaths.

The behavior of oceanic barotropic anticyclones was found to be very different, as expected. As the vortex approaches the slope by moving southwestward, fluid initially over the slope is displaced downhill and acquires positive relative vorticity. Thus, a vortex pair is formed that subsequently moves eastward, that is, away from the topography.

The presence of the strong western topography changes the cyclonic vortex evolution dramatically with respect to the purely vortex–wall interaction. In the latter case, the vortex slowly drifts southward, while leaking fluid to the north. Meanwhile, negative relative vorticity is created at the wall inducing the vortex to *rebound* in a dipole form (Zavala Sansón et al. 1999a). The strong topography inhibits the contact with the wall and triggers very different processes, as was shown.

As the numerical model was able to reproduce the most important aspects of the laboratory experiments it was possible to perform simulations with larger domains in order to test the influence of the other boundaries and the Rossby radiation. It was found that both of them have only a minor effect on the flow evolution. Also, additional simulations using isolated vortices as the initial condition showed only small qualitative differences with the present results (not shown here). Those differences are related with the greater filamentation induced by the oppositely signed vorticity ring of such vortices.

As far as the authors know, the interaction of mesoscale oceanic cyclones with a western slope has not been reported before in observational studies. The present study demonstrates the vortex behavior and structure due to barotropic effects that may be encountered during such interactions. More importantly, the present results are useful for gaining a better understanding of the physical mechanisms involved. For instance, the results concerning the behavior of a meandering current along a western continental slope compare reasonably well with observations on the southeast U.S. continental shelf, where elongated cyclones have been observed to form on the slope as a result of the meandering Gulf Stream (Miller and Lee 1995).

Acknowledgments. One of the authors (L.Z.S.) acknowledges financial support from the Consejo Nacional de Ciencia y Tecnología (CONACYT) and from Eindhoven University of Technology (TUE). The help of Jos van Geffen with the numerical code is also gratefully acknowledged.

REFERENCES

Baines, P. G., and R. L. Hughes, 1996: Western boundary current separation: Inferences from a laboratory experiment. *J. Phys. Oceanogr.,* **26,** 2576–2588.

Carnevale, G. F., R. C. Kloosterziel, and G. J. F. van Heijst, 1991: Propagation of barotropic vortices over topography in a rotating tank. *J. Fluid Mech.,* **233,** 119–139.

——, O. U. Velasco Fuentes, and P. Orlandi, 1997: Inviscid dipole-vortex rebound from a wall or coast. *J. Fluid Mech.,* **351,** 75–103.

Cushman-Roisin, B., J. A. Proehl, and D. T. Morgan, 1997: Barotropic thin jets over arbitrary topography. *Dyn. Atmos. Oceans,* **26,** 73–93.

Dalziel, S., 1992: DigImage. Image processing for fluid dynamics. Cambridge Environmental Research Consultants Ltd., 27 pp.

Grimshaw, R., D. Broutman, X. He, and P. Sun, 1994a: Analytical and numerical study of a barotropic eddy on a topographic slope. *J. Phys. Oceanogr.,* **24,** 1587–1607.

——, Y. Tang, and D. Broutman, 1994b: The effect of vortex stretching on the evolution of barotropic eddies over a topographic slope. *Geophys. Astrophys. Fluid Dyn.,* **76,** 43–71.

Kloosterziel, R. C., and G. J. F. van Heijst, 1991: An experimental study of unstable barotropic vortices in a rotating fluid. *J. Fluid Mech.,* **223,** 1–24.

LaCasce, J. H., 1998: A geostrophic vortex over a slope. *J. Phys. Oceanogr.,* **28,** 2362–2381.

Louis, J. P., and C. S. Smith, 1982: The development of the barotropic radiation field of an eddy over a slope. *J. Phys. Oceanogr.,* **12,** 56–73.

Masuda, A., K. Marubayashi, and M. Ishibashi, 1989: A laboratory experiment and numerical simulation of an isolated barotropic eddy in a basin with topographic β. *J. Fluid Mech.,* **213,** 641–655.

Miller, J. L., and T. N. Lee, 1995: Gulf Stream meanders in the South Atlantic Bight. 1. Scaling and energetics. *J. Geophys. Res.,* **100,** 6687–6704.

Nof, D., 1988: Draining vortices. *Geophys. Astrophys. Fluid Dyn.,* **42,** 187–208.

Orlandi, P., 1990: Vortex dipole rebound from a wall. *Phys. Fluids.,* **2A,** 1429–1436.

Smith D. C., IV, 1986: A numerical study of loop current eddy interaction with topography in the western Gulf of Mexico. *J. Phys. Oceanogr.,* **16,** 1260–1272.

——, and J. J. O'Brien, 1983: The interaction of a two-layer mesoscale eddy with bottom topography. *J. Phys. Oceanogr.,* **13,** 1681–1697.

van Geffen, J. H. G. M., 1998: NS-evol. Faculty of Technical Physics Internal Rep. R-1466-D, Eindhoven University of Technology, Netherlands, 152 pp. [Available from Fluid Dynamics Laboratory, Eindhoven University of Technology, 5600 MB Eindhoven, Netherlands.]

van Heijst, G. J. F., 1994: Topography effects on vortices in a rotating fluid. *Meccanica,* **29,** 431–451.

Zavala Sansón, L., G. J. F. van Heijst, and F. J. J. Janssen, 1999a: Experiments on barotropic vortex–wall interaction on a topographic β-plane. *J. Geophys. Res.,* **104,** 10 917–10 932.

——, and J. J. J. Doorschot, 1999b: Reflection of barotropic vortices from a step-like topography. *Il Nuovo Cimento C,* **22,** 909–929.